Chinese Journal of Catalysis 35 (2014) 1727–1739

available at www.sciencedirect.com

ScienceDirect

journal homepage: www.elsevier.com/locate/chnjc

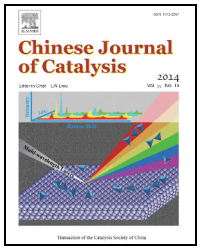

Article

Synthesis of mesoporous ZSM-5 using a new gemini surfactant as a mesoporous directing agent: A crystallization transformation process

Quanyi Wang [a,b,e], Yingxu Wei [a,*], Shutao Xu [a], Mozhi Zhang [a,e], Shuanghe Meng [a], Dong Fan [a,e], Yue Qi [a], Jinzhe Li [a], Zhengxi Yu [a], Cuiyu Yuan [a], Yanli He [a], Shuliang Xu [a], Jingrun Chen [a,e], Jinbang Wang [a], Baolian Su [b,c,#], Zhongmin Liu [a,d,§]

[a] *Dalian National Laboratory for Clean Energy, Dalian Institute of Chemical Physics, Chinese Academy of Sciences, Dalian 116023, Liaoning, China*
[b] *Laboratory of Inorganic Materials Chemistry (CMI), University of Namur (FUNDP), 61 rue de Bruxelles, B-5000 Namur, Belgium*
[c] *State key Laboratory of Advanced Technology for Materials Synthesis and Processing, Wuhan University of Technology, Wuhan 430070, Hubei, China*
[d] *State Key Laboratory of Catalysis, Dalian Institute of Chemical Physics, Chinese Academy of Sciences, Dalian 116023, Liaoning, China*
[e] *University of Chinese Academy of Sciences, Beijing 100049, China*

ARTICLE INFO

Article history:
Received 9 April 2014
Accepted 28 May 2014
Published 20 October 2014

Keywords:
Mesoporous ZSM-5
Dual-templating
Gemini surfactant
Inter-crystalline mesopore
Crystallization transformation

ABSTRACT

A new gemini surfactant, $[C_{18}H_{37}(CH_3)_2–N^+–(CH_2)_3–N^+–(CH_3)_2C_{18}H_{37}]Cl_2$ ($C_{18\text{-}3\text{-}18}$), has been successfully used as the mesopore directing agent in the hydrothermal synthesis of mesoporous ZSM-5 (MZSM-5). The synthesis of MZSM-5 was realized with a low temperature crystallization process at 130 °C. The amount of $C_{18\text{-}3\text{-}18}$ used in the synthesis affected the relative crystallinity and the textural properties of the obtained MZSM-5. Detailed investigation showed that the formation of MZSM-5 followed a crystallization transformation process. The use of $C_{18\text{-}3\text{-}18}$ resulted in the formation of mesoporous material during the early stage of the synthesis, which was converted into MZSM-5 crystals templated by tetrapropylammonium bromide to form the MFI phase. As the synthesis proceeded, the MZSM-5 crystals aggregated into particles by weak interactions. This work shows that $C_{18\text{-}3\text{-}18}$ can be used as a mesopore directing agent, which could provide a route for the synthesis of other mesoporous zeolites.

1. Introduction

Mesoporous ZSM-5 (MZSM-5), normally referred to ZSM-5 with both micropore and mesopore systems, is supposed to combine the benefits of each separate pore size regime and has great potential to improve the efficiency of zeolite catalysis, enhance the accessibility to active sites, and reduce the diffusion obstacle [1–4]. Therefore, considerable efforts have focused on the synthesis of MZSM-5.

A wide variety of synthesis strategies have been proposed to create mesopores in ZSM-5 crystals. Various post-treatment methods, including heat treatment [5], acid leaching [6–8], steaming treatment [6,7], alkaline leaching [9,10], and other chemical treatments [11], have proven to be efficient in creating mesopores in ZSM-5 crystals. Another strategy for the synthesis of ZSM-5 crystals containing mesopores is crystallization

* Corresponding author. Tel: 86-411-84379335; Fax: 86-411-84691570; E-mail: weiyx@dicp.ac.cn
# Corresponding Author. E-mail: bao-lian.su@unamur.be, baoliansu@whut.edu.cn
§ Corresponding author. Tel: 86-411-84379335; Fax: 86-411-84691570; E-mail: liuzm@dicp.ac.cn
This work was supported by the National Natural Science Foundation of China (21273230, 21273005, 21103176, 21103180).
DOI: 10.1016/S1872-2067(14)60128-5 | http://www.sciencedirect.com/science/journal/18722067 | Chin. J. Catal., Vol. 35, No. 10, October 2014

using a dual-templating method, which includes both ZSM-5 templates and mesopore structure directing agents. In the dual-templating method, both hard templates, such as carbon nanoparticles or nanotubes [12,13], poly(methyl methacrylate) (PMMA) nanospheres [14], nano $CaCO_3$ [15], and polymer beads [16], and soft templates, such as cationic surfactants (CTABs) [17,18], nonionic alkyl poly(ethylene oxide) surfactants [19], organosiliane [20], cationic polymer [21], silylated polymer [22], and natural products [23], have attracted considerable attention because of their high efficiency in creating mesopores in ZSM-5. Recently, Ryoo et al. [24–26] made progress in synthesizing MZSM-5 using an organic surfactant equipped with a multi-ammonium headgroup, which could serve as both a zeolitic template and a mesogenous structure directing agent. Synthesis methods involving the development of new surfactants for mesoporous zeolite synthesis are still of interest in the field of hierarchical materials.

In this study, we report a facile and highly efficient synthesis route to prepare MZSM-5 using a new gemini surfactant, $[C_{18}H_{37}(CH_3)_2–N^+–(CH_2)_3–N^+–(CH_3)_2C_{18}H_{37}]Cl_2$ ($C_{18\text{-}3\text{-}18}$), as the mesopore directing agent. Scheme 1 shows the structure model of $C_{18\text{-}3\text{-}18}$. To the best of our knowledge, the synthesis of MZSM-5 using $C_{18\text{-}3\text{-}18}$ as the mesopore directing agent has not been reported. The formation mechanism of MZSM-5 templated from $C_{18\text{-}3\text{-}18}$ is also discussed based on experimental observations.

2. Experimental

2.1. Chemicals and synthesis

All of the chemical reagents in this article ($NaAlO_2$ (41 wt% Al_2O_3), tetraethyl orthosilicate (TEOS, 98.0%,), tetrapropylammonium bromide (TPABr, 98.0%), NaOH (96.0%), and $C_{18\text{-}3\text{-}18}$ (95.0%)) were commercial products of analytical grade, and were used as received without further purification.

The MZSM-5 samples were synthesized with the hydrothermal method using $C_{18\text{-}3\text{-}18}$ as the mesogenous template and a gel with the molar composition of 40 SiO_2:1 Al_2O_3:20 NaOH: 10 TPABr:x $C_{18\text{-}3\text{-}18}$:7000 H_2O with different crystallization temperatures and times. In a typical synthesis procedure, 0.26 g $NaAlO_2$, 0.80 g NaOH, and 2.80 g TPABr were dissolved in 135 g H_2O. Then, 8.93 g TEOS and 3.33 g $C_{18\text{-}3\text{-}18}$ (here, x = 4) were added into the synthesis gel under agitation. After mixing, the synthesis gel was transferred into a 200 mL Teflon-lined stainless steel pressure vessel, sealed, and heated under autogenic pressure with vigorous stirring. After crystallization, the as-synthesized sample was centrifugally separated, washed, dried at 120 °C for 12 h, and calcined at 600 °C for 6 h. Herein, the sample synthesized at 150 °C for 36 h is denoted MZSM-5-A, the sample synthesized at 130 °C for 120 h is denoted MZSM-5-B, and the sample first synthesized at 120 °C for 48 h and then at 175 °C for 6 h is denoted MZSM-5-C. For comparison, conventional ZSM-5 was also synthesized starting from the synthesis gel with the same composition but without adding $C_{18\text{-}3\text{-}18}$, and this sample is referred to as ZSM-5. The crystallization conditions of ZSM-5 were 175 °C for 48 h.

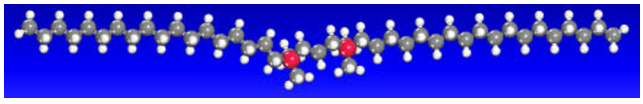

Scheme 1. Structure model of $[C_{18}H_{37}(CH_3)_2–N^+–(CH_2)_3–N^+–(CH_3)_2C_{18}H_{37}]Cl_2$.

2.2. Characterization

X-ray diffraction (XRD) patterns were obtained with a D/max-rb X-ray diffractometer, using Cu K_α radiation (λ = 1.5405 Å) at room temperature with instrumental settings of 40 kV and 40 mA. The relative crystallinity was calculated based on the intensity of the five peaks with 2θ = 22°–25°.

Scanning electron microscopy (SEM) images were obtained for morphological identification using a KYKY AMRAY-1000B scanning microscope. Transmission electron microscopy (TEM) images were obtained with a JEOL JEM-2000Ex electron microscope at 120 kV.

N_2 adsorption-desorption experiments were performed at –196 °C on a NOVA 4000 gas adsorption analyzer (Quantachrome Corp.). Each sample was evacuated at 130 °C for 1 h and then at 350 °C for 3 h before adsorption.

^{27}Al magic angle spinning (MAS) nuclear magnetic resonance (NMR) measurements were performed on a 600 MHz Bruker Avance III equipped with a 4 mm MAS probe. ^{27}Al MAS NMR spectra were recorded using one pulse sequence with a spinning rate of 12 kHz. 100 scans were accumulated with a π/8 pulse width of 0.75 μs and a 2 s recycle delay. The chemical shifts were referenced to $(NH_4)Al(SO_4)_2{\cdot}12\ H_2O$ at –0.4 ppm.

3. Results and discussion

3.1. Synthesis at different crystallization temperatures

The XRD patterns of the samples synthesized using different crystallization temperature routes are shown in Fig. 1 and compared with the XRD pattern of conventional ZSM-5. The intrinsic lattice structure of the MFI topology was observed for all samples, and no other phases were formed during the syn-

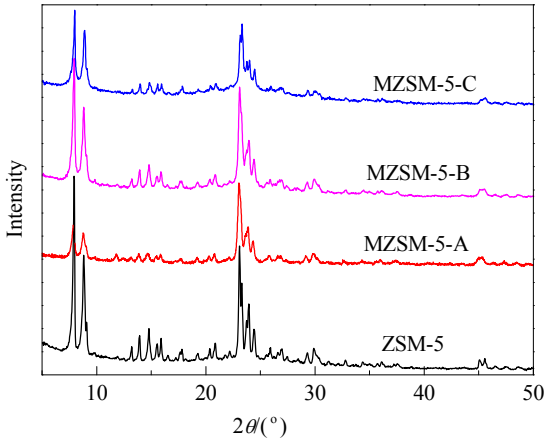

Fig. 1. XRD patterns of ZSM-5 and the MZSM-5 samples synthesized at different crystallization temperatures.

thesis. Furthermore, even starting from the gel with the same composition using dual templates (TPABr and $C_{18\text{-}3\text{-}18}$) there was still some difference in the relative crystallinity of the synthesized MZSM-5 samples, which can be attributed to the different crystallization temperatures. Among the three MZSM-5 samples, MZSM-5-A and MZSM-5-C had low relative crystallinity. MZSM-5-B had the highest relative crystallinity and very close to that of conventional ZSM-5, indicating that the crystallization procedure for MZSM-5-B (130 °C for 120 h) had the optimal conditions for the synthesis of MZSM-5.

The N_2 adsorption-desorption isotherms of ZSM-5 and the MZSM-5 samples are shown in Fig. 2(a). The curves of the pore size distribution, which were calculated from the adsorption branches using the BJH model, are shown in Fig. 2(b). As shown in Fig. 2(a), ZSM-5 shows a representative Type I (Langmuir) isotherm according to the classification of IUPAC, with no obvious increase in the adsorbed N_2 amount and no distinct hysteresis loop at high relative pressure, which is characteristic of microporous materials with no mesoporosity. This is verified by the BJH pore size distribution curve of ZSM-5 (Fig. 2(b)), where there is no obvious peak in the mesoporous range, indicating only microporosity in ZSM-5. As listed in Table 1, the BET surface area and total pore volume of ZSM-5 are 328 m^2/g and 0.16 cm^3/g, while the mesoporous surface area and pore volume are very low, only 59 m^2/g and 0.03 cm^3/g, respectively.

For the MZSM-5 samples, the N_2 adsorption-desorption isotherms are greatly different from that of conventional ZSM-5. As shown in Fig. 2(a), the N_2 adsorption-desorption isotherms of the MZSM-5 samples are mixed Type I and Type IV isotherms, indicating the existence of both microporosity and mesoporosity in the three samples (MZSM-5-A, MZSM-5-B, and MZSM-5-C) synthesized by the dual-templating method at different crystallization temperatures. The other important features include a dramatic increase in the adsorption amounts at high relative pressure compared with the conventional ZSM-5 isotherm. In addition, a hysteresis loop confirms the generation of mesopores. Because of the generation of mesopores in the three samples, their mesoporous surface areas and mesoporous volumes are larger than those of ZSM-5. However, the increase in mesoporosity of the MZSM-5 samples is accompanied with a decrease of microporosity (Table 1). The pore size distributions of the MZSM-5 samples calculated from the adsorption branches using the BJH model show a wide range of pore sizes, which suggests the possible generation of inter-crystalline mesopores. As shown in Fig. 2(b), the mesopore sizes of MZSM-5-A, MZSM-5-B, and MZSM-5-C vary from 2 to 100 nm. Most of the mesopores in MZSM-5-A and MZSM-5-C are around 50 nm, while the peak of mesopores around 50 nm in MZSM-5-B is relatively low intensity. However, the number of mesopores in the range 2 to 10 nm is significantly larger for MZSM-5-B than for MZSM-5-B and MZSM-5-C.

Table 1
Textural properties of conventional ZSM-5 and the MZSM-5 samples synthesized at different crystallization temperatures.

Sample	Surface area (m^2/g)			Pore volume (cm^3/g)		
	S_{BET}	S_{Meso}	S_{Micro}	V_{total}	V_{Meso}	V_{Micro}
ZSM-5	328	59	269	0.16	0.03	0.13
MZSM-5-A	254	133	121	0.55	0.49	0.06
MZSM-5-B	418	268	150	0.73	0.66	0.07
MZSM-5-C	279	141	138	0.38	0.32	0.06

The representative SEM images of ZSM-5 and the MZSM-5 samples are given in Fig. 3. Microporous ZSM-5 appears to be composed of crystals with different sizes from 0.6 to 1 μm. MZSM-5-A is also composed of crystals of different sizes. The larger crystals with a size of ~10 μm seem to be the aggregation of smaller crystals of ~1 μm. As shown in Fig. 3(e), MZSM-5-B is composed of different sized particles, and its enlarged image (Fig. 3(f)) shows that the grainy surface of MZSM-5-B is the aggregation of many small ZSM-5 crystals. In addition, it should be mentioned that the aggregation of ZSM-5 crystals into particles can induce the formation of some inter-crystalline mesopores in MZSM-5-B, which can be seen in Fig. 3(f). This result is consistent with the N_2 physical adsorption measurement. Correspondingly, Fig. 3(g) and (h) indicate that MZSM-5-C, like MZSM-5-A and MZSM-5-B, is composed of different sized particles, which are composed of small ZSM-5 crystals. Among the three MZSM-5 samples, MZSM-5-B has a

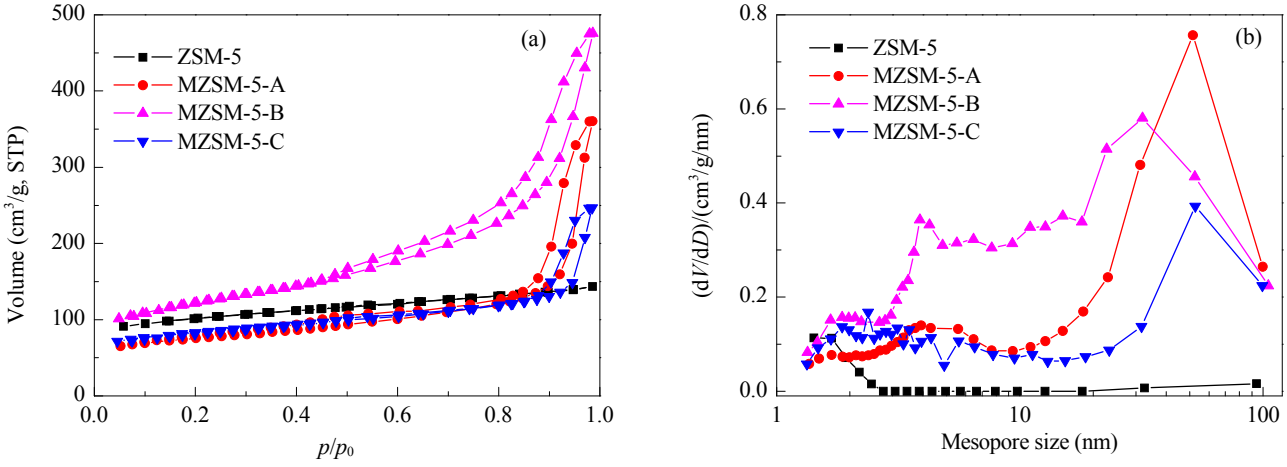

Fig. 2. N_2 adsorption-desorption isotherms (a) and pore size distributions (b) of conventional ZSM-5 and the MZSM-5 samples synthesized at different crystallization temperatures.

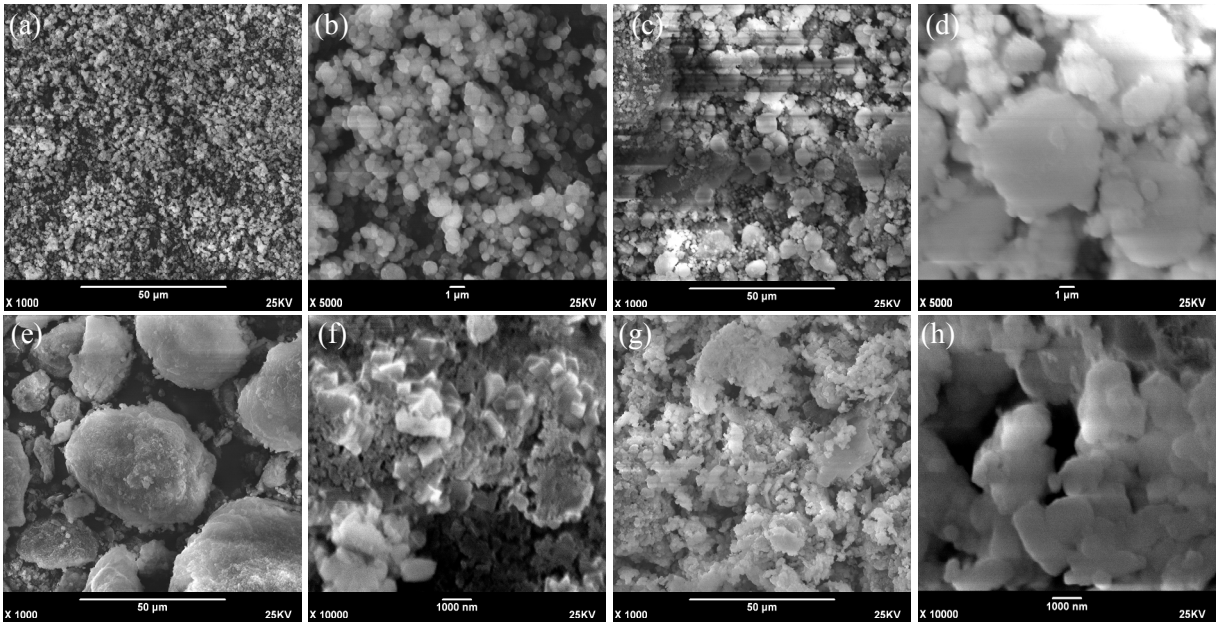

Fig. 3. SEM images of ZSM-5 and the MZSM-5 samples synthesized at different crystallization temperatures. (a) ZSM-5; (b) Enlargement of (a); (c) MZSM-5-A; (d) Enlargement of (c); (e) MZSM-5-B; (f) Enlargement of (e); (g) MZSM-5-C; (h) Enlargement of (g).

more regular morphology, which may result from the relatively low crystallization temperature.

Based on the characterizations mentioned above, it can be concluded that the different crystallization routes carried out at different temperatures affect the morphology and the textural properties of synthesized MZSM-5. A relatively low crystalline temperature, such as 130 °C, seems to be the optimal crystallization temperature for the synthesis of MZSM-5 with high mesoporous surface area, high mesoporous volume, and regular morphology, as well as good relative crystallinity from the formation of the MFI phase during the synthesis. The relatively low crystallization temperature required to synthesize MZSM-5 using $C_{18\text{-}3\text{-}18}$ as a mesopore directing agent may originate from its unique $-N^+-(CH_2)_3-N^+-$ group, which still needs further investigation.

3.2. *Effect of the amount of $C_{18\text{-}3\text{-}18}$*

The amount of mesoporous structure directing agent usually affects the relative crystallinity, morphology, and textural properties of the synthesized MZSM-5. Thus, the effect of the amount of $C_{18\text{-}3\text{-}18}$ was also investigated in the MZSM-5 synthesis following the optimized crystallization route confirmed in Section 3.1 (crystallization at 130 °C for 96 h). The molar composition of the starting gel was 40 SiO_2:1 Al_2O_3:20 NaOH:10 TPABr:*x* $C_{18\text{-}3\text{-}18}$:7000 H_2O, in which *x* represents the amount of $C_{18\text{-}3\text{-}18}$ used in the synthesis gel.

The XRD patterns of the samples synthesized using different amounts of $C_{18\text{-}3\text{-}18}$ are shown in Fig. 4. Even varying the amount of mesoporous structure directing agent, the intrinsic lattice structure of the MFI topology was identified for all four samples, and no other phases were formed during the synthesis of the MZSM-5 samples. Furthermore, when $C_{18\text{-}3\text{-}18}$ was added in amounts of x = 2 and 4, there was almost no difference in the relative crystallinity of the two synthesized MZSM-5 samples. When more $C_{18\text{-}3\text{-}18}$ was added (x = 6), the relative crystallinity of the synthesized MZSM-5 structure was higher than with x = 2 or 4. Further increasing the amount of $C_{18\text{-}3\text{-}18}$ (x = 8) resulted in a decrease of the relative crystallinity of the synthesized MZSM-5 sample compared with x = 6. This is usually observed during the synthesis of MZSM-5 using the dual-templating method. Under most circumstances, the two different templating systems, i.e., the ZSM-5 structure directing agent (TPABr) and the mesoporous template ($C_{18\text{-}3\text{-}18}$), work in a competitive rather than a cooperative manner. If too much $C_{18\text{-}3\text{-}18}$ is added into the synthesis gel, even though the mesoporous phase can be generated, the very slow formation of the MFI phase results in it being difficult to transform the generated mesoporous phase to crystallized ZSM-5. Therefore, more of the mesoporous phase remains, which results in a low relative crystallinity.

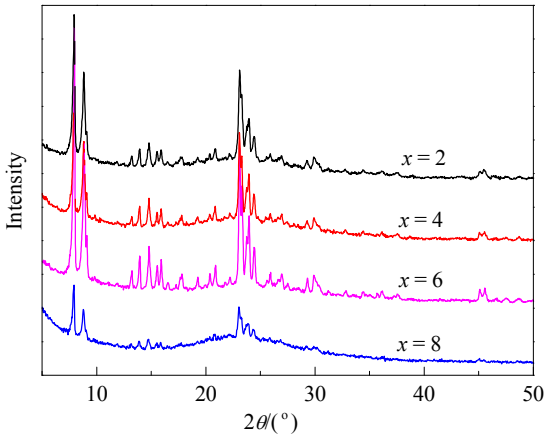

Fig. 4. XRD patterns of the MZSM-5 samples synthesized using different amounts of $C_{18\text{-}3\text{-}18}$.

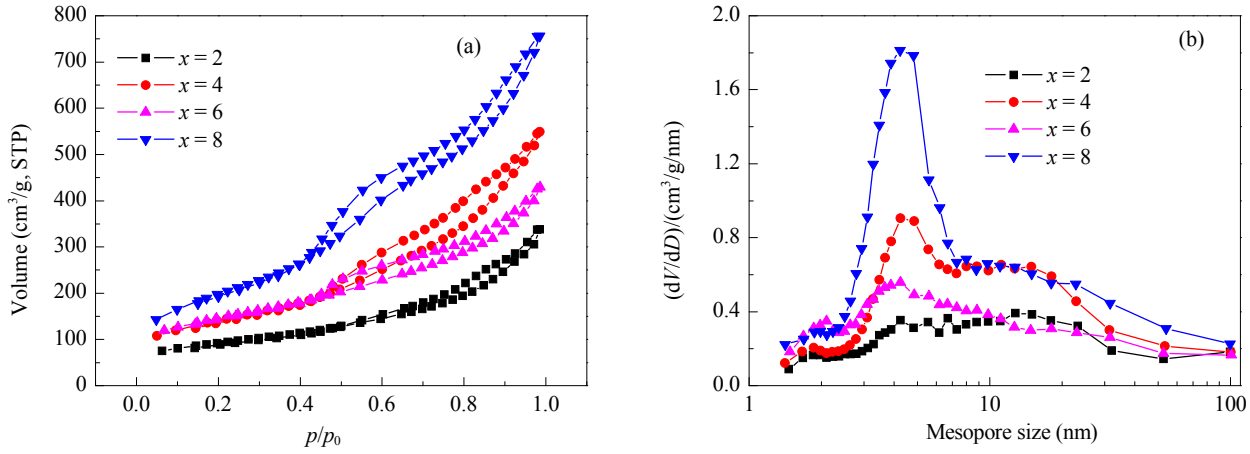

Fig. 5. N_2 adsorption-desorption isotherms (a) and pore size distributions (b) of the MZSM-5 samples synthesized using different amounts of $C_{18\text{-}3\text{-}18}$.

The N_2 adsorption-desorption isotherms, the pore size distribution curves, and textual properties of the samples synthesized using different amounts of $C_{18\text{-}3\text{-}18}$ are shown in Fig. 5 and Table 2. As shown in Fig. 5a, all of the N_2 adsorption and desorption isotherms of the MZSM-5 samples are mixed Type I and Type IV isotherms, indicating the coexistence of micropores and mesopores. With increasing added amount of $C_{18\text{-}3\text{-}18}$ from x = 2 to 6, the total surface area (S_{BET}) increased from 325 m^2/g to 515 m^2/g. Among the three samples, the total pore volume of the sample synthesized with x = 4 (0.82 cm^3/g) was higher than the other two samples (0.52 cm^3/g for x = 2 and 0.66 cm^3/g for x = 6), which may stem from its rich mesoporosity. The relatively low pore volume of the sample synthesized with x = 6 can be explained by the generation of more micropores, resulting in the loss of mesopores. Further increasing the amount of $C_{18\text{-}3\text{-}18}$ to x = 8, resulted in the obtained MZSM-5 having the highest surface area and pore volume among the four samples, which is because of the generation of a highly mesoporous structure. However, considering its very low relative crystallinity and microporous surface area, the addition of too much of the mesopore directing agent is not beneficial for the generation of MZSM-5.

The abovementioned results indicate that under the present experimental conditions, the addition of a moderate amount of $C_{18\text{-}3\text{-}18}$ during the synthesis (x = 4 and 6) favors the synthesis of MZSM-5 with good relative crystallinity and relatively good mesopore generation.

The pore size distributions of the four MZSM-5 samples (Fig. 5(b)) indicate that the generated mesopores have a wide range of sizes (2–30 nm) when adding a moderate amount of $C_{18\text{-}3\text{-}18}$ (x = 2, 4, and 6) into the synthesis gel. Increasing the amount of $C_{18\text{-}3\text{-}18}$ to x = 8 results in the generated mesopores having a narrow size range centered at 4 nm.

Table 2
Textural properties of the MSM-5 samples synthesized using different amounts of $C_{18\text{-}3\text{-}18}$.

$C_{18\text{-}3\text{-}18}$ amount	Surface area (m^2/g)			Pore volume (cm^3/g)		
	S_{BET}	S_{Meso}	S_{Micro}	V_{total}	V_{Meso}	V_{Micro}
x = 2	325	253	72	0.52	0.49	0.03
x = 4	491	389	102	0.82	0.78	0.04
x = 6	515	405	110	0.66	0.61	0.05
x = 8	720	698	22	1.16	1.15	0.01

3.3. Formation process of MZSM-5

To investigate the formation process of MZSM-5, the synthesis was carried out for different crystallization times using the same amount of $C_{18\text{-}3\text{-}18}$ (x = 4) at 130 °C. Samples were synthesized and characterized for crystallization times of 8, 24, 48, 72, 96, and 120 h. The samples synthesized for 96 and 120 h have been mentioned above, the sample with x = 4 in Section 3.2 and MZSM-5-B in Section 3.1.

The small-angle and the wide-angle powder XRD patterns of the samples synthesized for different crystallization times are shown in Fig. 6. When the synthesis was performed for 8 or 24 h, no diffraction peaks are present in the wide-angle powder XRD pattern of the solid samples. However, a peak is present in their small-angle powder XRD patterns, suggesting the two

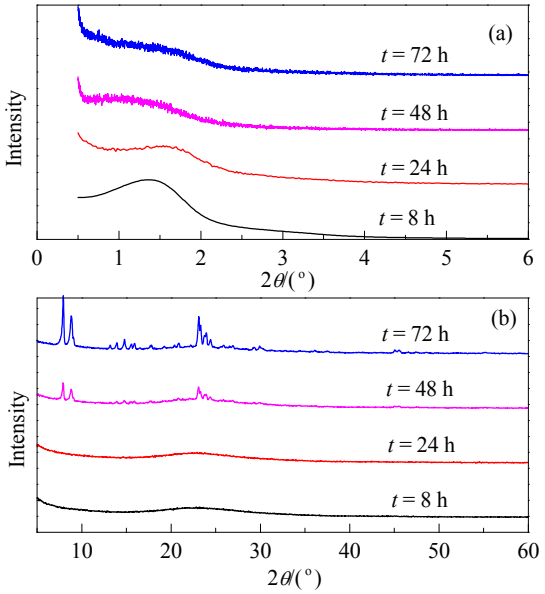

Fig. 6. Small-angle (a) and wide-angle (b) powder XRD patterns of samples synthesized for different crystallization times.

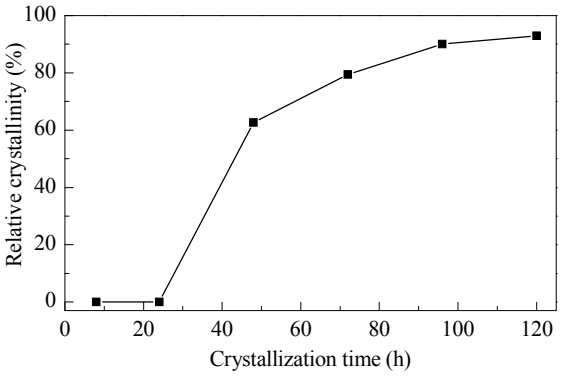

Fig. 7. Crystallization curve of MZSM-5 synthesized at 130 °C.

samples are mesoporous materials. For the samples synthesized for more than 24 h, ZSM-5 is detected as the only crystalline phase during the crystallization process. This indicates the slow crystallization character of ZSM-5 under the given experimental conditions, in which an induction period in the early stage is required for the crystallization process. Diffraction peaks of ZSM-5 become evident after crystallization for 48 h, and the intensity of the peaks greatly increases when increasing the crystallization time to 72 h.

The crystallization curve based on the relative crystallinity calculated from Fig. 6 is shown in Fig. 7. The reference sample used here is conventional ZSM-5, whose relative crystallinity was defined as 100%. During the initial 24 h, there is an induction period and no ZSM-5 phase forms. For a crystallization time of 48 h, the relative crystallinity sharply increases to 63%. Then, the relative crystallinity gradually increases from 63% to 93% with increasing crystallization time from 48 to 120 h.

N_2 adsorption-desorption experiments were conducted to investigate the change of the textural properties of the synthesized samples during the crystallization process. The N_2 adsorption-desorption isotherms and the pore size distribution curves of the samples synthesized at different crystallization times are shown in Fig. 8. All of the N_2 adsorption-adsorption isotherms of the samples crystallized for more than 8 h have a typical Type IV isotherm, indicating mesoporous structures. The pore size is centered at 4.5 nm. Mesopores with pore diameter greater than 10 nm are also present. When increasing the crystallization time to 24 h, the synthesized sample is still mostly mesoporous, although a small number of micropores are formed, as indicated in Fig. 8(b) and Table 3. The pore size distribution also changes, and more mesopores of ~20 nm in diameter are present. As the crystallization time is further increased to 48 and 72 h, the corresponding N_2 adsorption-desorption isotherms change and pore size distribution show a remarkable decrease in the number of ~4 nm diameter mesopores, and an increase in the number of ~30 nm diameter mesopores.

Table 3
Textural properties of samples synthesized for different crystallization times.

Crystallization time (h)	Surface area (m^2/g)			Pore volume (cm^3/g)		
	S_{BET}	S_{Meso}	S_{Micro}	V_{total}	V_{Meso}	V_{Micro}
8	690	690	0	1.07	1.07	0
24	668	624	44	1.22	1.21	0.01
48	548	508	40	1.16	1.15	0.01
72	502	431	71	0.84	0.81	0.03

The textural properties of the samples synthesized for different crystallization times are listed in Table 3. With the generation of the MFI phase in the synthesized samples, the microporous surface area and volume increase while the surface area and pore volume associated with the mesoporous surface decrease. S_{BET} and S_{Meso} of the samples decrease with increasing crystallization time while S_{Micro} tends to increase. The variation of the pore volume shows almost the same trend as that of the surface areas except for the slightly lower total pore volume at 8 h. From the XRD characterizations, both the samples synthesized for 8 and 24 h are mesoporous. The small difference in the pore volumes indicates that the mesoporosity developed during this period.

To clarify the structural change process of the samples synthesized for different crystallization times, TEM images were obtained. Figure 9 shows the TEM images of the samples synthesized for different crystallization times. As shown in Fig. 9(a), only mesoporous material with an irregular lamellar structure was formed during the initial 8 h, which is in good agreement with the XRD results (Fig. 6(a)). After synthesis for

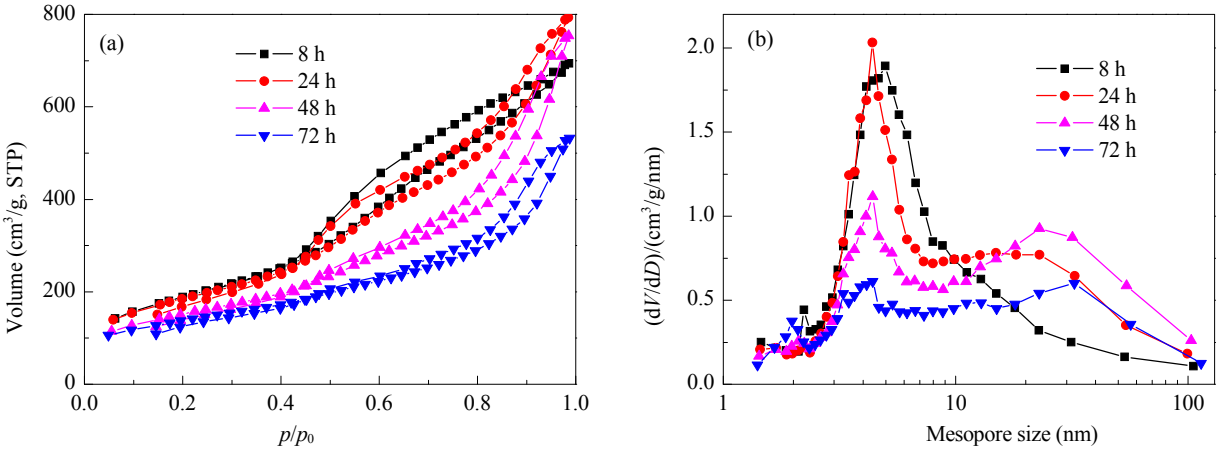

Fig. 8. N_2 adsorption-desorption isotherms (a) and pore size distributions (b) of samples synthesized at different crystallization times.

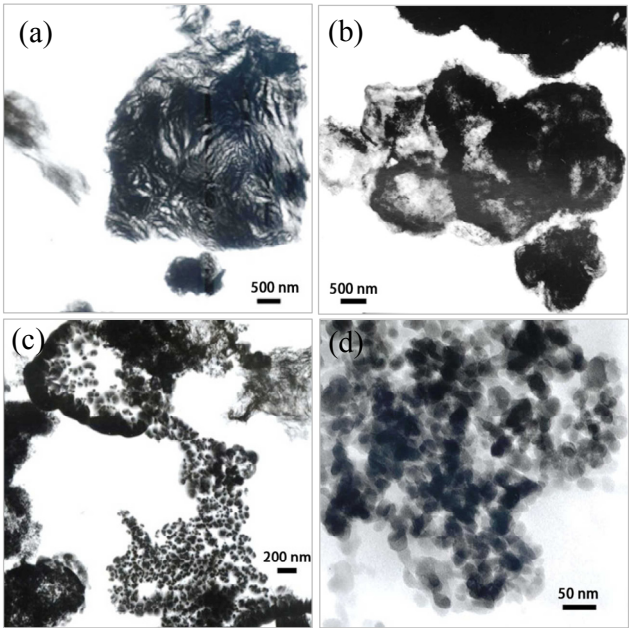

Fig. 9. TEM images of samples synthesized for crystallization times of 8 (a), 24 (b), 48 (c), and 72 h (d).

24 h, the obtained sample still retains the mesoporous phase, as indicated in the XRD pattern, while the corresponding TEM image (Fig. 9(b)) indicates that the sample grows into a hollow structure. This change in the structure confirms the development of mesopores during the synthesis period from 8 to 24 h, which may lead to the difference in pore volume (Table 3). Further increasing the crystallization time to 48 h leads to a rapid transformation from the mesoporous structure with hollow morphology to the crystalline phase. As shown in Fig. 9(c), a large number of crystals are observed, although the shell part of the hollow structure remains untransformed. Upon heating the synthesis gel for 72 h, there is no amorphous phase and only crystals are observed (Fig. 9(d)). In addition, the ZSM-5 crystals aggregate to form particles, which is consistent with the SEM results.

To obtain more information about the zeolite framework formation and the local coordination environment of Al species during the synthesis process, ^{27}Al MAS NMR experiments were conducted. Since the MFI phase was confirmed to form after crystallization for 48 h, only the samples synthesized for 8, 48, and 120 h were used for the ^{27}Al MAS NMR investigation.

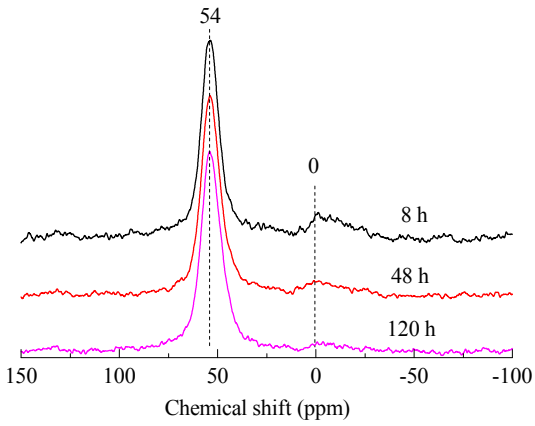

Fig. 10. ^{27}Al MAS NMR spectra of samples synthesized for crystallization times of 8, 48, and 120 h.

Figure 10 shows the ^{27}Al MAS NMR spectra of samples synthesized for crystallization times of 8, 48, and 120 h. Two peaks are present in the spectra of all three samples. The peak centered at ~54 ppm corresponds to tetrahedral Al of framework Al species. The other peak, centered at ~0 ppm with lower intensity, is ascribed to octahedral Al, which is normally associated with non-framework Al species. Furthermore, from Fig. 10, the peaks at ~54 ppm for all three samples have high intensity, which indicates that large amounts of tetrahedral Al are present in the ZSM-5 framework, even at the early stage of the synthesis (8 h). Furthermore, the intensity of the peak at ~0 ppm slowly decreased with the increase of the crystallization time from 8 to 120 h. This indicates that an increasing amount of octahedral Al in the non-framework Al species are converted into tetrahedral Al and located in the framework of the MZSM-5 with increasing crystallization time.

Based on the analysis of the results above, a possible mechanism to explain the formation of MZSM-5 using $C_{18\text{-}3\text{-}18}$ as a mesopore directing agent for the crystallization transformation process is shown in Scheme 2. During the early stage (Step I), a

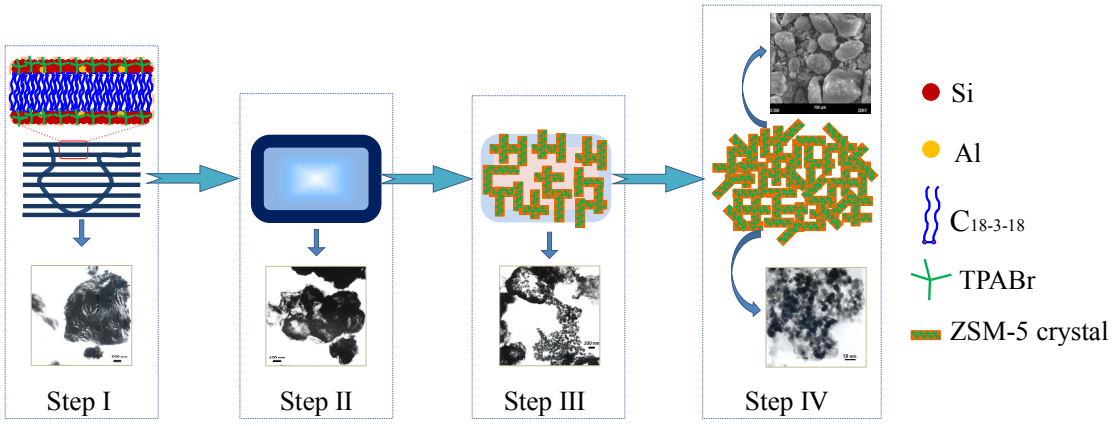

Scheme 2. Proposed formation process for the synthesis of MZSM-5 using $C_{18\text{-}3\text{-}18}$ as a mesoporous structure directing agent.

mesoporous irregular lamellar structure is formed from the starting synthesis gel under the structure directing function of $C_{18\text{-}3\text{-}18}$. The mesoporous phase then changes from the irregular lamellar structure to a hollow structure (Step II). As the hydrothermal synthesis proceeds (Step III), the mesoporous hollow structure crystallizes into ZSM-5 crystals (MFI phase) with the involvement of the TPABr microporous template. Finally, the generated ZSM-5 crystals grow and aggregate to form MZSM-5 particles with large diameter mesopores (>10 nm) between the crystal particles (Step IV), and the initially formed mesopores of ~4 nm in size are destroyed with crystallization.

4. Conclusions

In summary, MZSM-5 with inter-crystalline mesopores was successfully synthesized by a dual-templating hydrothermal method using a new gemini surfactant, $C_{18\text{-}3\text{-}18}$, as a mesopore directing agent. This synthesis method was confirmed to be effective at different crystallization temperatures. A low crystallization temperature, such as 130 °C, was better for the synthesis of MZSM-5 with good crystallinity, high mesoporous surface area, high mesoporous volume, and regular morphology. The relatively low crystallization temperature required may originate from the unique $-N^+-(CH_2)_3-N^+-$ group of the $C_{18\text{-}3\text{-}18}$ mesopore directing agent. The amount of $C_{18\text{-}3\text{-}18}$ used in the synthesis affected the relative crystallinity and the textural properties of the obtained MZSM-5. Optimizing the ratio of mesoporous directing agent ($C_{18\text{-}3\text{-}18}$) to microporous template (TPABr) ensured the synthesis of MZSM-5. Detailed investigation showed that the formation of MZSM-5 followed a crystallization transformation process. $C_{18\text{-}3\text{-}18}$ caused the formation of mesoporous material during the early stage, which was subsequently converted into MZSM-5 crystals by the function of TPABr as the template for the formation of the MFI phase. As the synthesis proceeded, the MZSM-5 crystals aggregate into particles by weak interactions. $C_{18\text{-}3\text{-}18}$ as a mesopore directing agent could be extended to the synthesis of other mesoporous zeolites.

Acknowledgment

B. L. Su acknowledges the Chinese Central Government for an “Expert of the State” position in the program of “Thousands Talents” and the Chinese Ministry of Education for a Changjiang Scholar position at the Wuhan University of Technology.

References

[1] Serrano D P, Aguado J, Escola J M, Rodríguez J M, Peral Á. *Chem Mater*, 2006, 18: 2462
[2] Chal R, Gérardin C, Bulut M, van Donk S. *ChemCatChem*, 2011, 3: 67
[3] Na K, Choi M, Ryoo R, *Micropor Mesopor Mater*, 2013, 166: 3
[4] Li X Y, Sun M H, Rooke J C, Chen L H, Sun B L. *Chin J Catal*, 2013, 34: 22
[5] Zhang C M, Liu Q, Xu Z, Wang K S. *Microporous Mesoporous Mater*, 2003, 62: 157

Graphical Abstract

Chin. J. Catal., 2014, 35: 1727–1739 doi: 10.1016/S1872-2067(14)60128-5

Synthesis of mesoporous ZSM-5 using a new gemini surfactant as a mesopore directing agent: A crystallization transformation process

Quanyi Wang, Yingxu Wei *, Shutao Xu, Mozhi Zhang, Shuanghe Meng, Dong Fan, Yue Qi, Jinzhe Li, Zhengxi Yu, Cuiyu Yuan, Yanli He, Shuliang Xu, Jingrun Chen, Jinbang Wang, Baolian Su *, Zhongmin Liu *
Dalian Institute of Chemical Physics, Chinese Academy of Sciences, China; University of Namur (FUNDP), Belgium; Wuhan University of Technology, China; University of Chinese Academy of Sciences, China

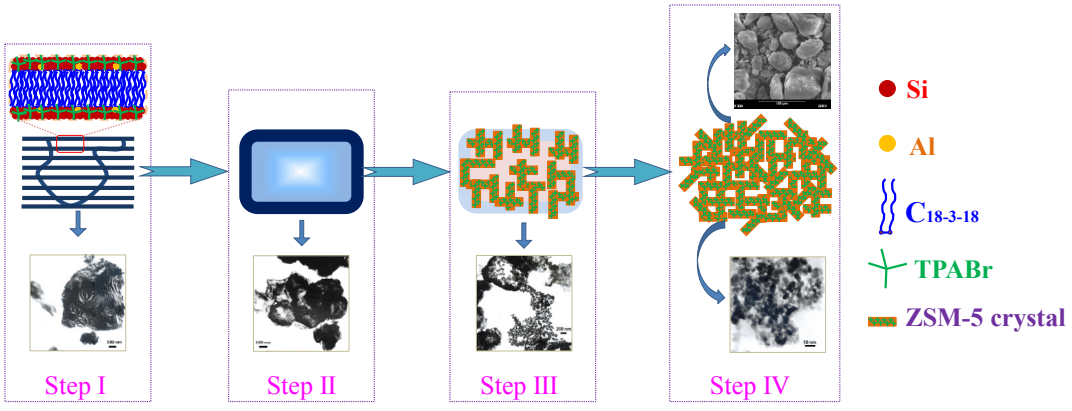

A new gemini surfactant, $[C_{18}H_{37}(CH_3)_2-N^+-(CH_2)_3-N^+-(CH_3)_2C_{18}H_{37}]Cl_2$ ($C_{18\text{-}3\text{-}18}$), has been successfully used to synthesize mesoporous ZSM-5 via a crystallization transformation process. The mesoporous material formed using the $C_{18\text{-}3\text{-}18}$ template during the early stage and was subsequently converted into mesoporous ZSM-5 crystals using tetrapropylammonium bromide as the template for the formation of MFI phase.

[6] Beers A E W, van Bokhoven J A, de Lathouder K M, Kapteijn F, Moulijn J A. *J Catal*, 2003, 218: 239
[7] Viswanadham N, Kumar M. *Microporous Mesoporous Mater*, 2006, 92: 31
[8] Song Y M, Ren N, Tang Y. *Chin J Catal*, 2012, 33: 192
[9] Groen J C, Peffer L A A, Moulijn J A, Perez-Ramirez J. *Chem Eur J*, 2005, 11: 4983
[10] Qi X L, Chen X M, Kong D J, Zheng J L, Yuan X H, Yang D Q. *Chin J Catal*, 2009, 30: 1197
[11] Triantafillidis C S, Vlessidis A G, Evmiridis N P. *Ind Eng Chem Res*, 2000, 39: 307
[12] Jacobsen C J H, Madsen C, Houzvicka J, Schmidt I, Carlsson A. *J Am Chem Soc*, 2000, 122: 7116
[13] Tao Y S, Kanoh H, Kaneko K. *J Am Chem Soc*, 2003, 125: 6044
[14] Zhao J J, Zhou J, Chen Y, He Q J, Ruan M L, Guo L M, Shi J L, Chen H R. *J Mater Chem*, 2009, 19: 7614
[15] Zhu H B, Liu Z C, Wang Y D, Kong D J, Yuan X H, Xie Z K. *Chem Mater*, 2008, 20: 1134
[16] Holland B T, Abrams L, Stein A. *J Am Chem Soc*, 1999, 121: 4308
[17] Zhu Y, Hua Z L, Zhou J, Wang L J, Zhao J J, Gong Y, Wu W, Ruan M L, Shi J L. *Chem Eur J*, 2011, 17: 14618
[18] Wang Q Y, Xu S T, Chen J R, Wei Y X, Li J Z, Fan D, Yu Z X, Qi Y, He Y L, Xu S L, Yuan C Y, Zhou Y, Wang J B, Zhang M Z, Su B L, Liu Z M. *RSC Adv*, 2014, 4:21479
[19] Zhou J, Hua Z L, Liu Z C, Wu W, Zhu Y, Shi J L. *ACS Catal*, 2011, 1: 287
[20] Serrano D P, García R A, Vicente G, Linares M, Procházková D, Čejka J. *J Catal*, 2011, 279: 366
[21] Song J W, Ren L M, Yin C Y, Ji Y Y, Wu Z F, Li J X, Xiao F S. *J Phys Chem C*, 2008, 112: 8609
[22] Wang H, Pinnavaia T J. *Angew Chem Int Ed*, 2006, 45: 7603
[23] Jin J J, Zhang X D, Li Y S, Li H, Wu W, Cui Y L, Chen Q, Li L, Gu J L, Zhao W R, Shi J L. *Chem Eur J*, 2012, 18: 16549
[24] Choi M, Na K, Kim J, Sakamoto Y, Terasaki O, Ryoo R. *Nature*, 2009, 461: 246
[25] Na K, Choi M, Park W, Sakamoto Y, Terasaki O, Ryoo R. *J Am Chem Soc*, 2010, 132: 4169
[26] Na K, Jo C, Kim J, Cho K, Jung J, Seo Y, Messinger R J, Chmelka B F, Ryoo R. *Science*, 2011, 333: 328

Page numbers refer to the contents in the print version, which include both the English and Chinese versions of the paper. The online version only has the English version. The pages with the Chinese version are only available in the print version.